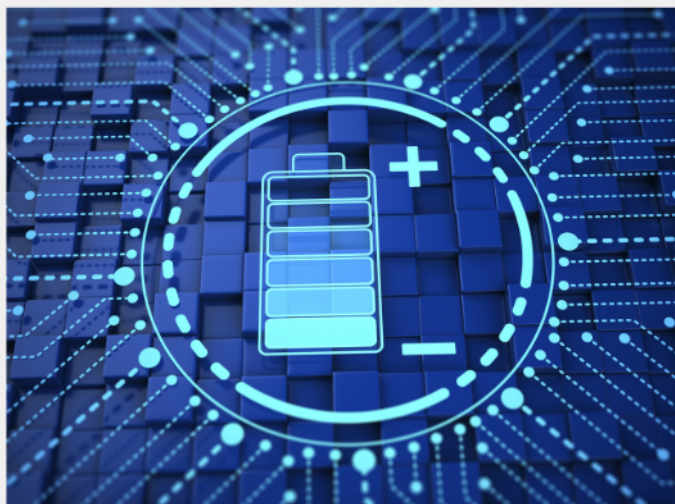




# Exploring the possibilities of increasing energy density and efficiency in rechargeable batteries

Download this complimentary article collection



The exponential rise in the need for better, more efficient power sources has sparked an incredible amount of research into batteries. A primary focus of research has been increasing the energy density of batteries, as it allows for lighter, more portable storage of energy. Lithium-ion batteries, for example, have a much higher energy density than conventional lead-acid batteries and can be used for various purposes, such as in electric vehicles.

This article collection provides a comprehensive list of references for new methods and technologies for increasing the energy density of batteries.

 **Metrohm**

**WILEY**

# Tough PEGgels by In Situ Phase Separation for 4D Printing

Zhenwu Wang, Matthias Heck, Wenwu Yang, Manfred Wilhelm, and Pavel A. Levkin\*

Polymer gels, consisting of cross-linked polymer network systems swollen by a solvent, show great potential in biomedicine, flexible electronics, and artificial muscles, due to their tissue-like mechanical properties. Due to the presence of a large amount of solvent, the improvement of the mechanical properties of the polymer gel is a challenge. Moreover, combining high toughness with useful properties, such as 3D printability or shape-memory, in one polymer gel system is even more challenging. In this study, a simple and efficient method is developed for the fabrication of tough polymer gels by polymerizing 2-hydroxyethyl methacrylate (HEMA) in a mixture of poly(ethylene glycol) (PEG) and poly(propylene glycol) (PPG). The polymerized elastic network presents distinct compatibility with PEG (compatible) and PPG (poorly compatible), resulting in in-situ phase separation at the microscale. The resulting phase-separated gel demonstrates high strength (8.0 MPa), favorable fracture strain (430%), and large toughness (17.0 MJ m<sup>-3</sup>). The separated hard phase with a high glass transition temperature (75 °C) endows the whole soft polymer gel with the property of shape memory at room temperature. Finally, the fabrication of tunable tough PEGgels is combined with 3D printing as well as with shape memory properties, demonstrating the use of PEGgels for 4D printing.

## 1. Introduction

Soft materials, due to their tissue-like mechanical properties, show great potential as materials for applications as diverse as tissue engineering, flexible electronics, bio-adhesives, or soft robotics.<sup>[1–4]</sup> Soft materials with various chemical functionalities, electrical properties, and mechanical properties have been developed to meet these engineering demands.<sup>[5–7]</sup> However, engineered soft materials still typically suffer from poor mechanical properties, resulting in unsatisfied reliability and premature failure under harsh conditions.<sup>[8]</sup> Hierarchical structures, commonly found in nature, for example, in plants, molluscs, tissues, etc., have been proven to enhance the mechanical properties,<sup>[9]</sup> where breaking the material with hierarchical structures requires more energy per unit volume than the one with the single structure.<sup>[10]</sup> Thus, creating a hierarchical structure across multiple length scales ranging from nanoscale to microscale by combining materials with

contrasting mechanical properties is an efficient strategy to achieve enhanced mechanical properties. Many studies have demonstrated that hard fillers at nanoscales, such as carbon materials<sup>[11]</sup> or metal particles,<sup>[12]</sup> can largely improve the mechanical properties of soft materials, through the formation of hierarchical structures within a soft matrix.<sup>[13]</sup> In situ formation of hard domains at the nano- and/or micro-scale within soft materials, similarly to the hierarchical structures formed in natural materials, can avoid the problem of mixing and compatibility with fillers.<sup>[14]</sup>


Polymer gels, consisting of cross-linked polymer networks infused with a mobile solvent,<sup>[15]</sup> are becoming one of the most promising soft materials due to the high customizability of their performance.<sup>[16]</sup> The internal structure of the gel, which is strongly influenced by its solvent affinity, determines its physical properties, such as optical, electrical, or mechanical.<sup>[17]</sup> A gel immersed in a good solvent swells extensively, usually becoming transparent and elastic. Gels immersed in poor solvents shrink, usually showing opacity due to internal phase separation triggered by the exchange of a good solvent by the poor one. Nevertheless, these separated phases were shown to efficiently enhance the toughness of polymer gels, especially at the micro/nanoscale.<sup>[14,18,19]</sup> Abundant efforts are devoted to designing tough polymer gels by means of phase separation, which usually involves laborious processing such as solvent exchange,<sup>[20]</sup> multistep syntheses,<sup>[21]</sup> and post-freezing

Z. Wang, P. A. Levkin  
Institute of Biological and Chemical Systems-Functional  
Molecular Systems (IBCS-FMS)  
Karlsruhe Institute of Technology (KIT)  
Hermann-von-Helmholtz-Platz 1, 76344 Eggenstein-Leopoldshafen,  
Germany  
E-mail: levkin@kit.edu

M. Heck, M. Wilhelm  
Institute for Chemical Technology and Polymer Chemistry (ITCP)  
Karlsruhe Institute of Technology (KIT)  
Kaiserstr 12, 76131 Karlsruhe, Germany

W. Yang  
Institute of Nanotechnology (INT)  
Karlsruhe Institute of Technology (KIT)  
Hermann-von-Helmholtz-Platz 1, 76344 Eggenstein-Leopoldshafen,  
Germany

P. A. Levkin  
Institute of Organic Chemistry (IOC)  
Karlsruhe Institute of Technology (KIT)  
Kaiserstr 12, 76131 Karlsruhe, Germany

 The ORCID identification number(s) for the author(s) of this article can be found under <https://doi.org/10.1002/adfm.202300947>.

© 2023 The Authors. Advanced Functional Materials published by Wiley-VCH GmbH. This is an open access article under the terms of the Creative Commons Attribution License, which permits use, distribution and reproduction in any medium, provided the original work is properly cited.

DOI: 10.1002/adfm.202300947

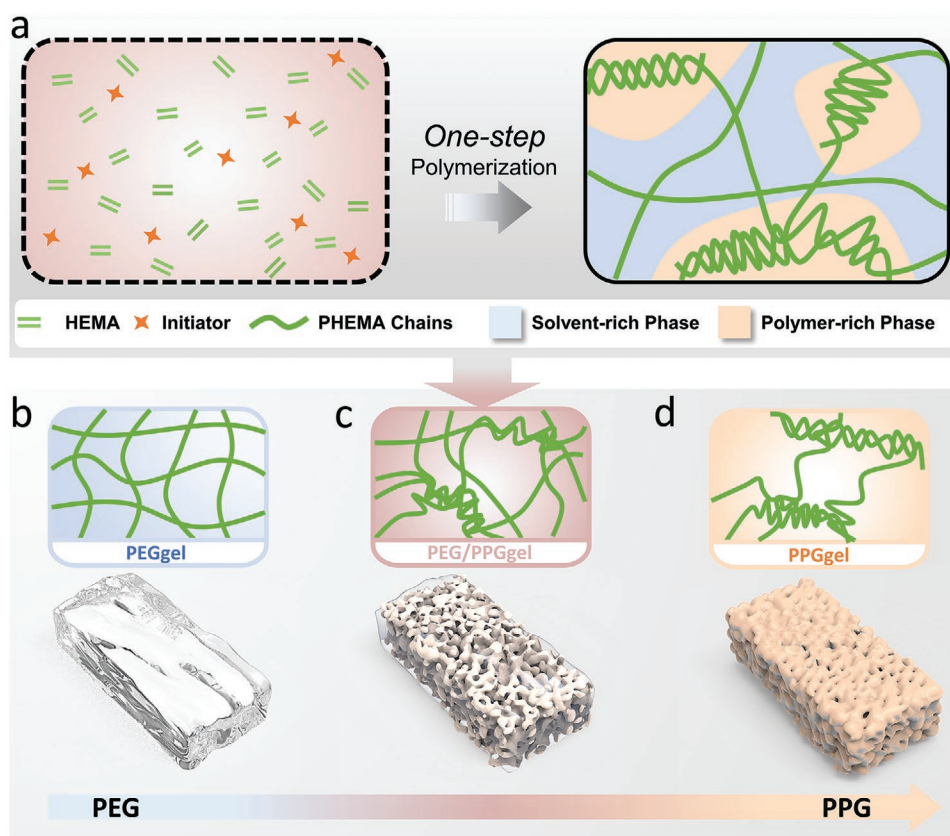


**Figure 1.** a) Schematic illustrations of in situ phase-separated polymer gels based on mixed oligomer solvents. b) When pure PEG is used as a (good) solvent, polymerization of HEMA leads to PEGgel – a uniform, transparent, and elastic material. c) When HEMA is polymerized in the presence of a mixture of PEG (good solvent) and PPG (poor solvent), in situ phase separation leads to an extremely tough gel (PEG/PPGgel) due to a hierarchical structure with interconnected soft and stiff domains. Soft domains connect the stiff domains to form an extremely tough gel. d) In 100% PPG (poor solvent), the phase separation is more pronounced, leading to larger PHEMA-rich hard domains surrounded by a continuous PPG-rich phase.

casting.<sup>[22]</sup> These shortcomings result in dimensional instability and poor processability, severely limiting further applications of phase-separated gels.

In this article, we demonstrate a facile one-step strategy to fabricate phase-separated gels by polymerizing monomers in a mixture of both good and poor solvents. After polymerization, the mixed solvents have the opposite effect on the formed polymer chains. At the excess of a good solvent, the polymer network is swollen in the solvent without phase separation, demonstrating soft and elastic properties. Increasing the fraction of a poor solvent leads to the formation of hard polymer-rich phase-separated domains surrounded by soft solvent-rich domains. Due to the good compatibility of the two solvents, the separation of soft and hard domains happens at the nano/micro scale, forming the hierarchical structures. In this study, 2-hydroxyethyl methacrylate (HEMA), poly(ethylene glycol) (PEG), and poly(propylene glycol) (PPG) were selected as the monomer, good solvent, and poor solvent, respectively (**Figure 1**). The phase separation endows the polymer gel with high strength (8.0 MPa) and outstanding toughness (170 MJ m<sup>-3</sup>). Another advantage of this method is its compatibility with 3D printing. Finally, we demonstrate that the phase separation and formation of hard polymer domains with a high glass transition temperature results in shape memory properties.

## 2. Results and Discussion

### 2.1. Concept of Phase-Separated Gel

As a demonstrator, poly(2-hydroxyethyl methacrylate) (PHEMA) was selected as the polymer network. All samples were produced by mixing 60 wt.% of 2-hydroxyethyl methacrylate, corresponding solvents (PEG, PEG/PPG, or PPG), and a photoinitiator with a pre-defined ratio (Table S1, Supporting Information). For comparability reasons, PEG and PPG of a similar average molecular weight were used ( $M_{n,PEG} \approx 400 \text{ g mol}^{-1}$ ,  $M_{n,PPG} \approx 425 \text{ g mol}^{-1}$ ). The mixtures were polymerized under UV light (5 mW cm<sup>-2</sup>, 366 nm, room temperature) for 30 min to form the PEGgel, the PEG/PPGgel or the PPGgel. Surprisingly, the three gels exhibited strong differences in both optical and mechanical properties. For a consistent description of the samples, we name them as “H<sub>x</sub>E<sub>y</sub>P<sub>z</sub>”, where H<sub>x</sub>, E<sub>y</sub>, and P<sub>z</sub> refer to the wt%/10 of the PHEMA (in the whole prepolymer solution), PEG (in the mixed solvent), and PPG (in the mixed solvent), respectively (Table S1, Supporting Information). Since PEG is a good solvent for PHEMA, the produced PEGgel (H<sub>6</sub>E<sub>10</sub>P<sub>0</sub>) is transparent, soft, elastic, and does not show signs of phase separation (**Figure 2a**). By contrast, PPG has lower compatibility with PHEMA due to its slightly higher hydrophobicity, which leads



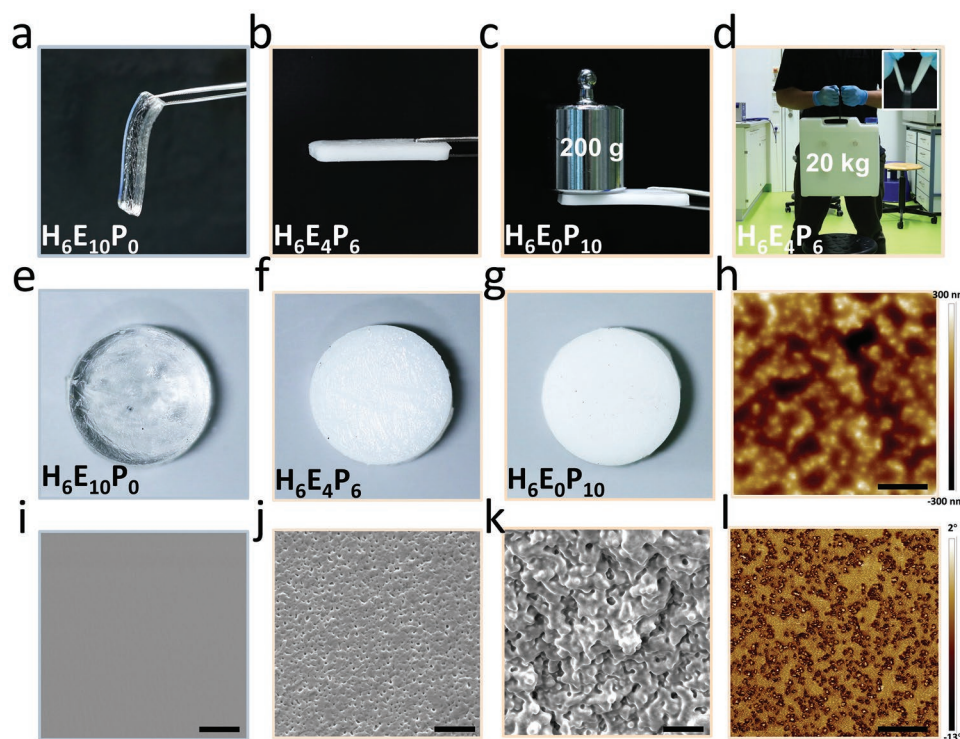


**Figure 2.** Overview and structural characterization of the phase-separated gel. a–c) Photographs of PEGgel ( $H_6E_{10}P_0$ ), PPGgel ( $H_6E_0P_{10}$ ), and PEG/PPGgel ( $H_6E_4P_6$ ). The size of these three gel samples is  $3 \times 15 \times 38$  mm. a)  $H_6E_{10}P_0$  is soft and flexible, achieving natural bending and sagging. b)  $H_6E_4P_6$  can support itself without bending. c)  $H_6E_0P_{10}$  behaves stiff and can hold 200 g weight without bending. d)  $H_6E_4P_6$  can lift 20 kg weight without damage (size:  $3 \times 15 \times 38$  mm). e–g) Photos of phase-separated gels with different solvent ratios, showing decreasing transparency/increasing light scattering with increasing content of PPG. The diameter of all samples is 10 mm. i–k) SEM image of phase-separated gels with different solvent ratios (i –  $H_6E_{10}P_0$ , j –  $H_6E_0P_{10}$ , k –  $H_6E_4P_6$ ). h) topographic AFM image and l) AFM phase image of  $H_6E_4P_6$ , collected simultaneously (field of view  $20 \mu\text{m} \times 20 \mu\text{m}$ ). All scale bars are  $5 \mu\text{m}$ .

to phase separation and a mechanically much harder opaque PPGgel (Figure 2,  $H_6E_0P_{10}$ ). Interestingly, by varying the ratio between PEG and PPG it is possible to fine-tune the mechanical properties of the produced polymer gel through the variation of the extent of phase separation. For example, a 40:60 (wt.%) mixture of PEG:PPG as solvent leads to a gel ( $H_6E_4P_6$ ) combining both the elasticity of PEGgel and the strength of PPGgel. A piece of such a gel (cross-section:  $3 \times 15$  mm) can, on the one hand, bend and also lift 20 kg weight without damage (Figure 2b). Polymerization-induced phase separation (Figure 2e–g) is evidenced by the white appearance of the produced polymer gel. UV–vis spectra (Figure S1, Supporting Information, cuvette thickness:  $300 \mu\text{m}$ ) show that with the increasing fraction of PPG, the average transmittance at wavelengths between 400 and 800 nm decreased from 99% ( $H_6E_{10}P_0$ ) to 39% ( $H_6E_0P_{10}$ ), indicating an increase in the average size of phase-separated domains along with the increase of the PPG fraction, leading to stronger light scattering. Characterization of the polymer gels by SEM also confirms this result. For  $H_6E_{10}P_0$ , the topography of the cross-section is smooth and uniform (Figure 2i), suggesting a homogeneously dispersed network. In  $H_6E_0P_{10}$ , the polymer-rich micrometer-sized domains are clearly separated from the surrounding solvent-rich phase (Figure 2k). SEM of  $H_6E_4P_6$  shown in Figure 2j also exhibits phase separation, the hard polymer-rich domains being, however, mixed or connected with soft solvent-rich domains. By using atomic force microscopy (AFM), similar

results were obtained (Figure S2, Supporting Information). Topographic AFM images of  $H_6E_{10}P_0$  and  $H_6E_0P_{10}$  showed distinct morphologies, the former being smooth and the latter rough. The  $H_6E_4P_6$  also had a rough morphology but smaller polymer-rich domains than the  $H_6E_0P_{10}$ , showing a separated phase structure on the length scale of microns (Figure 2h,l). To exclude the influence of polymer crystallization, wide-angle X-ray scattering was performed to investigate the nanostructure of the polymer gels (Figure S3, Supporting Information). It confirmed that all polymer gels based on PEG and PPG solvents have an amorphous structure without diffraction peaks. This indicates that the polymer-rich domains mainly depend on the aggregation of polymer chains in poor solvents rather than crystallization. This was additionally confirmed by differential scanning calorimetry (DSC) measurements on the pure PEG and PPG as well as on the respective gels (Figure S4, Supporting Information). For the pure PEG and PPG, melting peaks of crystallites in these polymers were observed at 6.5 and 5.5 °C, respectively. However, the crystallinity of these polymers in the polymer gel was completely suppressed and no melting peaks could be observed at all.

## 2.2. Mechanical Performance of Phase-Separated Gel

To further investigate the effect of a liquid phase on the mechanical properties of the polymer gels, we varied the

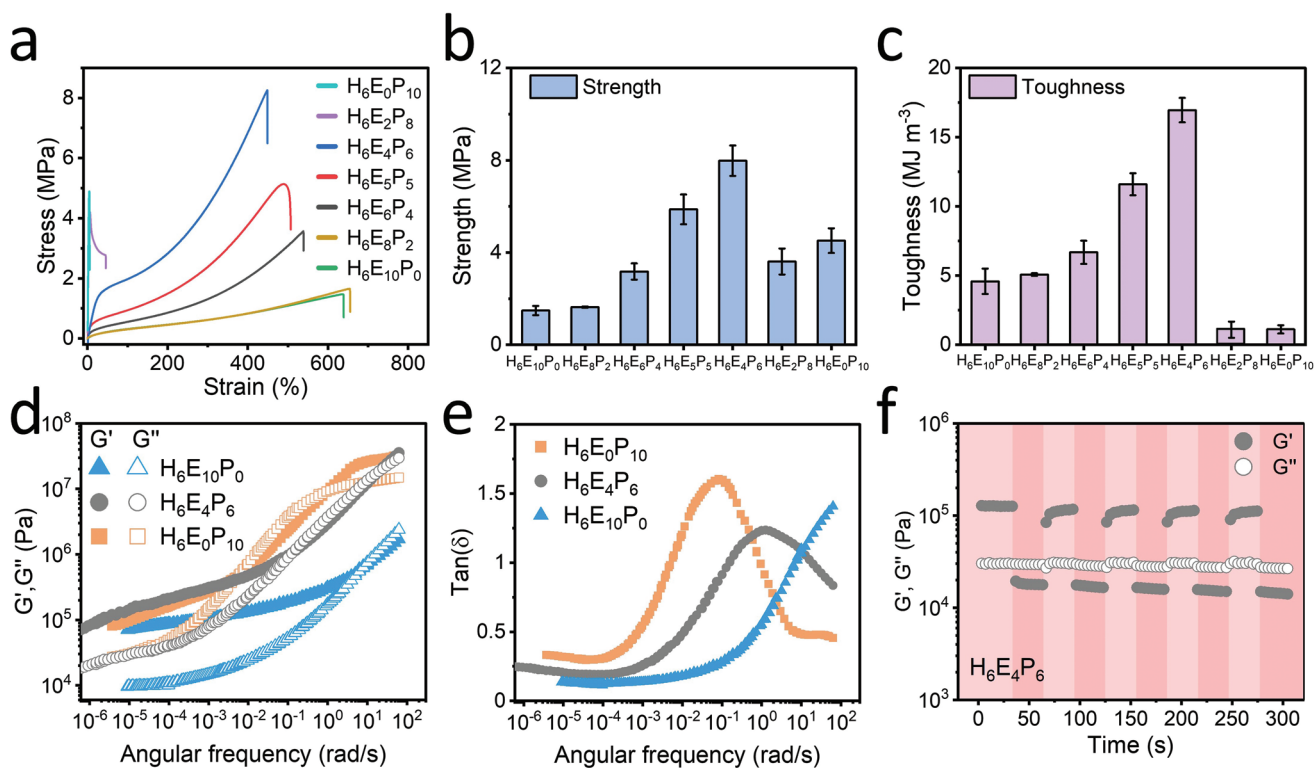


**Figure 3.** Mechanical properties of the phase-separated PEG/PPG polymer gels. a) Representative stress-strain curves of polymer gels with different ratios between PEG and PPG used as solvents. b) Strength and c) toughness of polymer gels with different compositions of PEG and PPG. Data represent the mean  $\pm$  standard deviation ( $n = 3$ ). d) Frequency dependence of the storage shear modulus ( $G'$ ) and the shear loss modulus ( $G''$ ) for H<sub>6</sub>E<sub>10</sub>P<sub>0</sub>, H<sub>6</sub>E<sub>4</sub>P<sub>6</sub>, and H<sub>6</sub>E<sub>0</sub>P<sub>10</sub> for a reference temperature of 30 °C. In the frequency sweep tests, the angular frequency was increased from 1 to 10 Hz at specified temperatures (from 30 to 160 °C, 10 °C for one step) with the shear strain of 0.5%. e) Angular frequency dependence of  $\tan \delta$  for the samples H<sub>6</sub>E<sub>10</sub>P<sub>0</sub>, H<sub>6</sub>E<sub>4</sub>P<sub>6</sub>, and H<sub>6</sub>E<sub>0</sub>P<sub>10</sub>. f)  $G'$  and  $G''$  of H<sub>6</sub>E<sub>4</sub>P<sub>6</sub> under continuous strain with alternate small oscillation strain ( $\gamma = 0.1\%$ ) and large one ( $\gamma = 60\%$ ) at 120 °C with an angular frequency of 10 rad s<sup>-1</sup>.

volume fraction of PPG, thereby efficiently achieving tunability of the mechanical properties of the phase-separated gel. The representative tensile stress-strain curves correspond to the polymer gels containing the same fraction of HEMA (60 wt.%) and varying in the solvent compositions (Figure 3a–c). The determination of the monomer ratio (60 wt.%) is discussed in the supporting information (Figure S5, Supporting Information). The PEGgel (H<sub>6</sub>E<sub>10</sub>P<sub>0</sub>), containing only PEG as the solvent, is soft and elastic with a low elastic modulus of 0.71  $\pm$  0.08 MPa, normal fracture stress of 1.48  $\pm$  0.20 MPa, and high fracture elongation of 650%  $\pm$  72%.

Upon increasing the content of PPG, phase separation occurs, and the fraction and size of polymer-rich domains increase in the polymer gels, making the polymer gels stronger and less elastic than H<sub>6</sub>E<sub>10</sub>P<sub>0</sub> (Figure S6, Supporting Information). When the fraction of PPG in the PPG/PEG mixture is less than 60 wt.%, the phase-separated gel is still soft and elastic, with fracture elongation higher than 400%. When the fraction of PPG reaches 80 wt.%, the gel becomes glass-like at room temperature, showing an abrupt increase in the elastic modulus from 12.8  $\pm$  3.9 MPa (H<sub>6</sub>E<sub>4</sub>P<sub>6</sub>) at 60 wt.% PPG to 29.1  $\pm$  4.2 MPa (H<sub>6</sub>E<sub>2</sub>P<sub>8</sub>) at 80 wt.% PPG and a sudden decrease in fracture elongation at break from 430%  $\pm$  28% (H<sub>6</sub>E<sub>4</sub>P<sub>6</sub>) to 6.4%  $\pm$  0.3% (H<sub>6</sub>E<sub>2</sub>P<sub>8</sub>), respectively. Such a hardening phenomenon results from the increased polymer-rich domains

in polymer gels. By further increasing the PPG fraction in the solvent to 100 wt.%, the polymer gel (H<sub>6</sub>E<sub>0</sub>P<sub>10</sub>) becomes stiff and brittle with a high elastic modulus of 124  $\pm$  21 MPa, fracture stress of 4.51  $\pm$  0.54 MPa, and very small fracture elongation of 4.8%  $\pm$  0.4%. Since toughness depends on the elongation and strength, the H<sub>6</sub>E<sub>4</sub>P<sub>6</sub> showing the highest fracture stress (8.0  $\pm$  0.7 MPa) and high fracture strain (430%  $\pm$  28%) demonstrates outstanding toughness (17.0  $\pm$  0.9 MJ m<sup>-3</sup>), which is 3.7 times higher than for H<sub>6</sub>E<sub>10</sub>P<sub>0</sub> (4.58  $\pm$  0.92 MJ m<sup>-3</sup>) and 15.5 times higher than for H<sub>6</sub>E<sub>0</sub>P<sub>10</sub> (1.1  $\pm$  0.3 MJ m<sup>-3</sup>). Notably, this simultaneous improvement of strength and toughness usually conflicts with material design, where the enhancement of strength usually comes with a large decrease in fracture strain. In phase-separated gels, the polymer-rich domains deform to dissipate energy for raising strength while the solvent-rich domains prevent the gel from early fracture showing high toughness.<sup>[23]</sup> In a pure PEG environment, the PHEMA networks are highly solvated by PEG, where few hydrogen bonds form between the PHEMA chains since solvent separates the polymer chains, resulting in soft and stretchable H<sub>6</sub>E<sub>10</sub>P<sub>0</sub>. Conversely, in 100% PPGgel (H<sub>6</sub>E<sub>0</sub>P<sub>10</sub>), phase separation leads to the formation of polymer-rich domains where the polymer networks are poorly solvated with prevailing inter PHEMA hydrogen bonds and entanglements, which results in a stiff and brittle bulk material. Here, we demonstrate that it is possible to fine-tune the amount

of poorly solvated domains (stiff, glass-like) and highly solvated domains (elastic, gel-like) in the same network mechanical by varying the ratio between the good (PEG) and poor (PPG) solvents, which in turn allows us not only to control the properties of the material but also to achieve a material combining both large toughness and high strength.

The dynamic responsive properties of the phase-separated gel were investigated by using a strain-controlled rotational rheometer. According to oscillatory strain sweep tests (Figure S7, Supporting Information), the linear viscoelastic regions of  $H_6E_{10}P_0$ ,  $H_6E_4P_6$ , and  $H_6E_0P_{10}$  exhibit a high dependence on the content of hard domains. With the decrease of the PPG fraction, the linear viscoelastic region increases from a strain amplitude of  $\gamma_0 = 1\%$  ( $H_6E_{10}P_0$ ) to 2% ( $H_6E_4P_6$ ) and 9% ( $H_6E_0P_{10}$ ) at the same angular frequency ( $10 \text{ rad s}^{-1}$ ) and temperature ( $120 \text{ }^\circ\text{C}$ ). Then, the frequency-dependent mechanical modulus of the three gels was determined in the linear viscoelastic regime. The rheological master curves describe the storage modulus ( $G'$ ), loss modulus ( $G''$ ), and loss factor ( $\tan \delta$ ) at a reference temperature of  $30 \text{ }^\circ\text{C}$  in dependence of the angular frequency ( $\omega$ ) are presented in Figure 3d,e.  $H_6E_4P_6$  and  $H_6E_0P_{10}$  exhibit a region ( $G'' > G'$ ), which might be attributed to the presence of separated domains. In contrast, for  $H_6E_{10}P_0$   $G'' > G'$  in nearly the whole investigated frequency range and a crossover of the moduli is just observed close to the highest frequencies, which were investigated ( $10^1 \text{ rad s}^{-1}$ ). Thus, the region ( $G'' > G'$ ) shifts to lower angular frequencies with the presence of hard domains.  $H_6E_0P_{10}$ , the sample with many hard domains, additionally presents a region at angular frequencies above  $0.1 \text{ rad s}^{-1}$ , in which  $G' > G''$  again. Additionally,  $G'$  of all samples is rather constant in the low-frequency region ( $\omega \rightarrow 0$ ). This results from the strong physical cross-links as well as multiple hydrogen bonds in the gel network, which prevent the network chains from reptation.<sup>[24]</sup> To quantify the relative energy-dissipation of a material,  $\tan \delta$  is a quantitative parameter. As the fraction of stiff domains increases, the peak of  $\tan \delta$  shifts to the low-frequency region (Figure 3e) as a clear response to the different local mobility of the investigated samples. This result is in accordance with the hypothesis that the separated stiff domains play a dominant role in the energy dissipation in polymer gels.

Rheological analyses were further used to demonstrate the recovery properties of phase-separated gels. Strain amplitude sweep experiments were performed to determine the viscoelastic region of the samples, and the critical strain of the samples were found to be  $\gamma_0 = 0.1\%$  and 60% at  $120 \text{ }^\circ\text{C}$  with an angular frequency of  $10 \text{ rad s}^{-1}$ , respectively, according to the performance under the previous strain sweep test. In Figure 3f and Figure S7 (Supporting Information), the  $G'$  values of all samples were found to decrease rapidly above the critical strain, indicating the nonlinear behavior of the gel network. For  $H_6E_{10}P_0$ , the value of  $G'$  decreased from  $\approx 53$  to  $\approx 2.5$  kPa after the strain amplitude increased from  $\gamma_0 = 0.1\%$  to 60%, indicating an impaired network. After decreasing the amplitude back to 0.1%,  $G'$  of  $H_6E_{10}P_0$  takes around 20 s to recover to the value of 40 kPa. For  $H_6E_4P_6$ , the original value of  $G'$  is  $\approx 125$  kPa, then the recovery process takes 15 s to achieve the recovery of  $G'$  from 18 kPa (at  $\gamma_0 = 60\%$ ) back to  $\approx 120$  kPa (at  $\gamma_0 = 0.1\%$ ). For  $H_6E_0P_{10}$ , the time for recovery (12 s) is slightly shorter than for  $H_6E_4P_6$ . According to such continuous switch tests between

small and large strain amplitudes, the improvement in recovery properties from the separated stiff domains is confirmed.

### 2.3. 4D Printing of Phase-Separated Gels

Shape-memory polymer gel can deform and then by applying a stimulus, will return to its previous shape. Such stimulus-responsive materials have shown a broad application prospect in various fields covering biomedical devices, soft robotics, and 4D printing.<sup>[25]</sup> Specifically, the shape-memory polymer gel possesses a permanent shape at room temperature, deforms at high temperatures, and retains the deformed temporary shape after cooling with the help of an external force. By reheating, it can return from a deformed temporary shape to a permanent shape.<sup>[26]</sup> Thermally-induced shape memory polymers often utilize the existence of several glass transition temperatures ( $T_g$ ) of the material to switch between a temporarily deformed shape and the set-permanent shape. Generally, above the  $T_g$ , the material becomes soft and rubbery, allowing it to be easily deformed or programmed. The deformed shape can be solidified by cooling the material below the  $T_g$  while maintaining the deformation.<sup>[27]</sup> Due to the existence of high  $T_g$  components, the shape-memory polymer gels have limitations in terms of their mechanical performance, which significantly constrains their application ranges. Also, the direct 3D printing of such stimulus-responsive materials is a challenge. Here, we hypothesized that locally separated and mechanically different domains could enable PEG/PPG gels to acquire shape-memory properties. Due to the existence of abundant hard domains, the phase-separated polymer gel is able to keep the programmed shape of the whole specimen after cooling to room temperature under deformation. The soft domains can maintain the elasticity of the material and prevent the occurrence of fractures in the polymer gel during the deformation.<sup>[28]</sup> Also, the 3D printability and good mechanical properties of phase-separated polymer gels can guarantee for various applications.

In order to test this idea, we performed the shape-memory test on polymer gels with different solvent compositions ( $H_6E_{10}P_0$ ,  $H_6E_4P_6$ , and  $H_6E_0P_{10}$ ) in Figure 4. At  $100 \text{ }^\circ\text{C}$ , approximately  $25 \text{ }^\circ\text{C}$  above the  $T_g$  of PHEMA in these samples, all three polymer gels became soft and could be folded to make a temporary shape. After cooling to  $25 \text{ }^\circ\text{C}$  and removing the external pressure, the  $H_6E_{10}P_0$  was unable to keep the temporary shape and recovered back to the original straight shape directly. On the contrary,  $H_6E_4P_6$  and  $H_6E_0P_{10}$  remained in their temporary shape, due to the presence of hard polymer-rich domains. After heating to  $100 \text{ }^\circ\text{C}$ ,  $H_6E_4P_6$  and  $H_6E_0P_{10}$  recovered to the original straight shape automatically, demonstrating the shape-memory effect. Notably,  $H_6E_4P_6$  with both soft and hard domains remained intact after the shaperecovery, while  $H_6E_0P_{10}$  with only hard domains cracked during the deformation. The cracks of  $H_6E_0P_{10}$  probably result from a combination of the brittleness of the cold material and temperature gradients in the sample during the heating process. During the heating processing, some parts of the sample became soft and started to unfold first, while other parts (middle of the sample) were still rigid and brittle. Such differences in mechanical properties within one sample combined with forces exerted on the material due



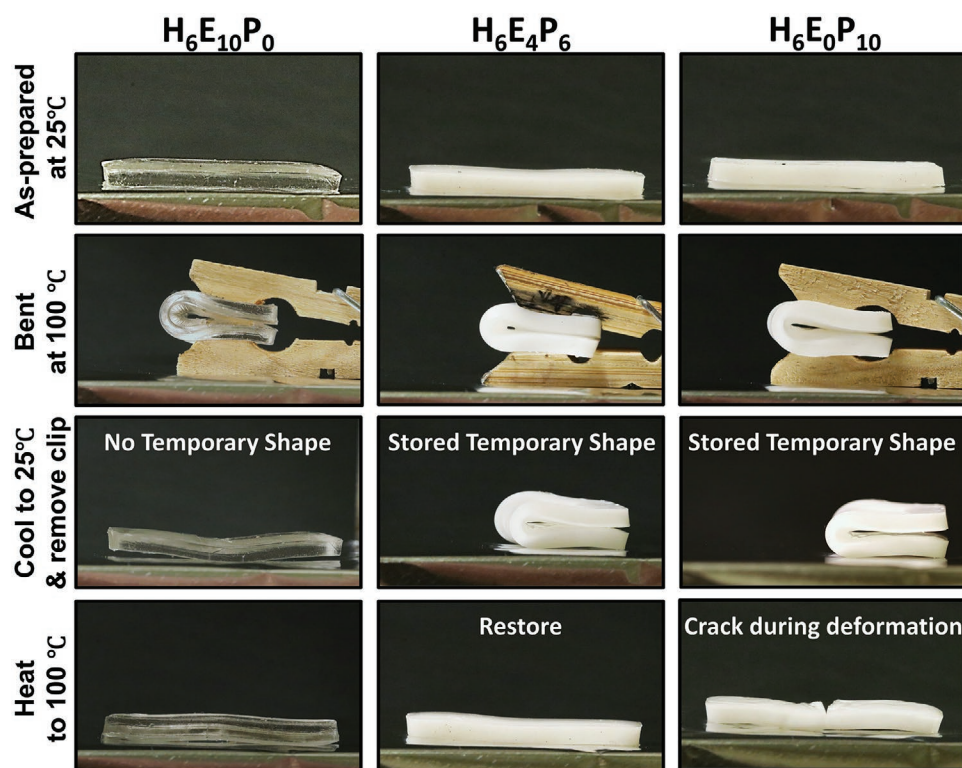


**Figure 4.** Shape-memory effect of the polymer gels with different solvent compositions. From left to right:  $H_6E_{10}P_0$ ,  $H_6E_4P_6$ , and  $H_6E_0P_{10}$ . At 100 °C, all three polymer gels are soft and can be folded to take a temporary shape. After cooling to 25 °C and removing the clip, the  $H_6E_{10}P_0$  recovered to the original shape without showing a shape-memory effect. On the contrary,  $H_6E_4P_6$  and  $H_6E_0P_{10}$  kept their temporary shape. After heating again to 100 °C,  $H_6E_4P_6$  and  $H_6E_0P_{10}$  recovered to the original shape automatically, demonstrating the shape-memory effect. Importantly,  $H_6E_0P_{10}$ , consisting of all hard domains, cracked during the deformation. The  $H_6E_4P_6$ , owning both soft and hard polymer-rich domains, remained intact after the shape recovery. The size of these three gel samples is 3 × 15 × 38 mm.

to the shape memory properties caused cracks. For  $H_6E_4P_6$ , the soft domains in the polymer gels could withstand the deformation, which effectively prevents crack formation. According to the result of differential scanning calorimetry (DSC), the  $H_6E_4P_6$  has two glass transition temperatures (Figure S8, Supporting Information), including a low  $T_{g1}$  of −44 °C and a high  $T_{g2}$  of 75 °C. These two temperatures mainly originate from the soft solvent-rich domains and the hard polymer-rich domains, respectively, as proved by the DSC traces obtained from  $H_6E_{10}P_0$  and  $H_6E_0P_{10}$ , respectively (Figure S8, Supporting Information). Thus, the undamaged shape-memory behavior of  $H_6E_4P_6$  can be demonstrated as below: 1) the gel was deformed (or “programmed”) at an elevated temperature above  $T_{g2}$  (100 °C) and cooled back to room temperature to preserve the programmed shape with the help of the hard polymer-rich domains. 2) The hard polymer-rich domains became rubbery and provided a driving force for the elastic recovery of the polymer chains, when the gel was heated above  $T_{g2}$ . 3) The gel lost the previously programmed shape and recovered to the original shape above  $T_{g2}$ , showing the shape-memory behavior. 4) The soft domains in the gel maintained the elasticity of the material and avoided fracture of the gel during the deformation. The thermal stability was further confirmed by thermogravimetric analysis (TGA). As evident from Figure S8 (Supporting Information), the TGA plot of  $H_6E_4P_6$  presented a negligible weight loss (<3%) up to 190 °C, demonstrating a wide operation window.

3D printing, an essential rapid manufacturing technique, can form arbitrary 3D structures directly, which greatly expands the application prospects of the materials and opens the possibility for rapid prototyping.<sup>[29,30]</sup> The simple one-step photopolymerization for the fabrication of our phase-separated gels is compatible with 3D printing by digital light processing (DLP). Thus, we could 3D print  $H_6E_4P_6$  into various complex shapes (Figure 5). The produced structures demonstrate the white appearance confirming the in situ phase separation during the printing.

In order to demonstrate a combination of the 3D printability with shape-memory behavior, we printed a hexagonal hollow egg-shaped structure using  $H_6E_4P_6$  composition, which was then “programmed” at 100 °C (Figure 5a) and cooled down to room temperature. The new shape was stable at room temperature. Heating the structure to 80 °C resulted in a quick recovery to the original shape in 20 s (Figure 5a; Movie S1, Supporting Information). Moreover, a quadruped model was directly printed and programmed into a lying-down state at room temperature. After heating over 80 °C, the quadruped model can stand by itself (Figure 5b; Movie S2, Supporting Information). We also designed and printed a quadruped model to achieve a more complex action. From the folded status, the small item could turn itself over and stand in the designed direction (Figure 5c; Movie S3, Supporting Information). Furthermore, due to the high strength of the phase-separated gel, the printed

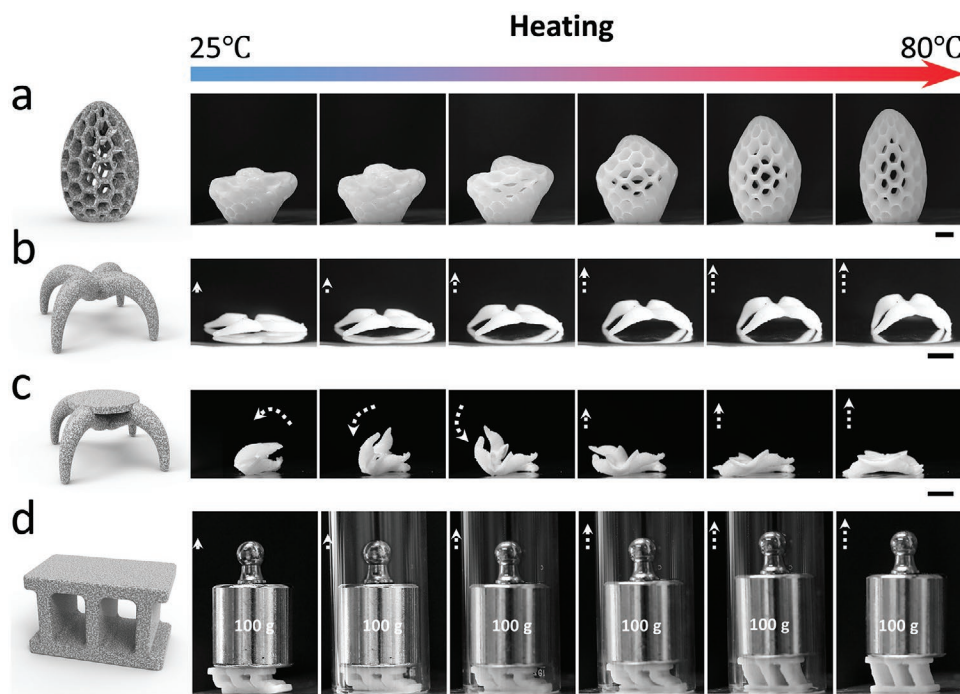


**Figure 5.** 4D printing of the phase-separated gel ( $H_6E_4P_6$ ). a) The 3D printed hexagonal hollow egg-shaped structure recovered from the collapsed state back to the original, showing the shape-memory behaviour. b) The 3D-printed quadruped model can stand by itself upon heating to 80 °C. c) The 3D-printed quadruped model with a small table can turn itself over and stand up after heating. d) The printed actuator can jack up to 100 g after heating, which is 116 times of its own weight (0.86 g). The samples with complex 3D structures were prepared by a DLP 3D printer using the  $H_6E_4P_6$  polymer mixture (Table S2, Supporting Information). The left column is the model designed for printing. All scale bars are 5 mm.

soft actuator could lift 100 g during heating, which is 116 times its own weight of 0.86 g (Figure 5d; Movie S4, Supporting Information). Such a combination of superb mechanical properties and 4D printability demonstrates the great potential of phase-separated gels in various soft machines such as medical devices, wearable devices, and soft robots. Compared with traditional shape memory devices based on simple planar or tubular geometries, 3D printed devices can efficiently expand functionalities such as directional deformation and versatile integration, while intimately meeting complex modeling needs.<sup>[31]</sup>

### 3. Conclusion

In summary, we developed a simple and efficient method for the fabrication of tough phase-separated polymer gels with the possibility of fine-tuning the mechanical properties of the material simply by varying the ratio between PEG and PPG solvents used in the polymerization mixture. We demonstrate that the addition of PPG to the HEMA-PEG mixture leads to an in situ phase separation and formation of micrometer-sized stiff polymer-rich domains, resulting in the toughening of the material. During deformation, the stiff polymer-rich phase mainly dissipates the energy, while the soft solvent-rich phase maintains large elongation. The resulting phase-separated polymer gel ( $H_6E_4P_6$ ) demonstrates high strength (8.0 MPa), favorable fracture strain (430%), and large toughness ( $170 \text{ MJ m}^{-3}$ ) at room temperature. In addition, we demonstrate the possibility

of combining in situ phase separation with 3D printing, which allows us to print 3D objects possessing enhanced mechanical properties due to the phase-separated nature of the PEG/PPG gel materials. Finally, the separated phases endow the polymer gel with a shape memory property, which in combination with 3D printability will be very interesting for creating various soft machines, soft actuators, or wearable electronics with tunable mechanical properties. Moreover, the proposed solvent-based method is not restricted to the materials mentioned above and can be used in conjunction with other design methods to fabricate polymer gels with tailored properties, which suggests its broad applicability. Such a simple and efficient strategy, combined with 3D printability and shape-memory properties, offers fundamental and extensible advanced functional materials, and should further inspire the design of novel soft materials and broaden their applications.

### 4. Experimental Section

**Materials:** Hydroxyethyl methacrylate and 2-hydroxy-2-methylpropiophenone (I1173) were purchased from Sigma-Aldrich (Darmstadt, Germany). Poly(ethylene glycol) (PEG) ( $M_n = 380\text{--}420 \text{ g/mol}$ ) and poly(propylene glycol) (PPG) ( $M_n = 425 \text{ g/mol}$ ) were purchased from Thermo Fisher (Schwerte, Germany). Both PEG and PPG were hydroxyl-terminated. All chemicals were used as received.

**Preparation of Phase-Separated Gels:** All samples were prepared via UV-induced one-pot sequential polymerization. HEMA, PEG, PPG, and the photo-initiator were mixed in brown bottles with designed ratios and vortex stirred for 2 min, obtaining transparent and uniform solutions. Moreover, the samples were initiated under 366 nm UV light



(5 mW cm<sup>-2</sup>) for 30 min. The specific prepolymer compositions are shown in Table S1 (Supporting Information).

**Mechanical Characterization:** The samples were tested using an AGS-X Universal tester (Shimadzu Inc., Japan). Three samples were prepared for each tensile experiment. For tensile tests, the tested samples were shaped into dumbbells with 1–2 mm thickness, 2 mm width, and 10 mm length. The tensile speed was set at 100 mm min<sup>-1</sup>. Three samples were tested as parallel samples.

The fracture energy was measured by pure shear tests.<sup>[15,32]</sup> Two identical samples with the same size in the tensile test were loaded under the sample setup as a pair to obtain one fracture energy value. One was notched, and the other one was unnotched. For the notched samples, an initial 20% width was cut in the middle of the long edge towards the center of the samples, and the specimen was loaded at a strain rate of 100 mm min<sup>-1</sup>. All specimens had microstructure alignment parallel to the height direction. The critical strain ( $\epsilon_c$ ) for notched samples was obtained from the strain at maximum stress. The unnotched pairing samples were subsequently loaded over  $\epsilon_c$ . The fracture energy ( $\Gamma$ ) was obtained by multiplying the area under the stress–strain ( $\sigma$ – $\epsilon$ ) curve of the unnotched specimens with the length of the sample ( $L$ ) as  $\Gamma = L \int_0^{\epsilon_c} \sigma d\epsilon$ .

The rheological properties were measured with an ARES-G2 Rheometer (TA Instruments, USA). The disc-shaped samples with a thickness of ≈1 mm and a diameter of 13 mm were adhered to the plates with superglue (UHU, Germany). The master curves were obtained by time-temperature superposition (TTS) at a reference temperature of 30 °C. During the frequency sweep tests, the angular frequency was increased from 1–10 Hz at specified temperatures (from 30 to 160 °C, 10 °C for one step) with the shear strain in the mechanical linear regime (0.5%). Other details of rheological measurements were mentioned in the main text.

**Material Characterization:** The transmission of the samples was measured using a UV–vis spectrometer (Lambda 35, Perkin Elmer) with a wavelength range of 400–800 nm. The thickness of the samples was 300 μm. Three samples were tested parallel, and every sample was scanned 24 times. The WAXS measurement was performed with a Bruker D8 Advance (Cu K<sub>α1</sub> radiation,  $\lambda = 1.54056$  Å). The Differential scanning calorimetry (DSC) measurements were performed on a TA DSC 2500 instrument in sealed 40 μL aluminum crucibles under a nitrogen atmosphere. Samples with 3–5 mg were analyzed using a heat/cool/heat cycle with a heating or cooling rate of 20 °C min<sup>-1</sup>. In this cyclic thermal measurement, the samples were heated from room temperature to 250 °C, cooled to –90 °C and reheated to 250 °C. The glass transition temperature ( $T_g$ ) was determined in the second heating run to eliminate possible interference from the polymer's thermal history.

## Supporting Information

Supporting Information is available from the Wiley Online Library or from the author.

## Acknowledgements

Z.W. thanks the China Scholarship Council (CSC) for the Ph.D. scholarship. The work was further supported by the Helmholtz program BIFTM. M.H. thanks the support of German Research Foundation (DFG, Wi 1911/22-1). Furthermore, the authors thank the support of the Helmholtz Program “Materials Systems Engineering” and KIT-Center-Projekt softNeuro 2020 (FE.5450.0014.5096). The authors thank Michael Pollard for editing the manuscript. P.A.L. thanks DFG's Heisenbergprofessur grant (406232485, LE 2936/-9-1) and Germany's Excellence Strategy 2082/-1-390761711 (Excellence Cluster “3DMM2O”).

Open access funding enabled and organized by Projekt DEAL.

## Conflict of Interest

The authors declare no conflict of interest.

## Data Availability Statement

The data that support the findings of this study are available from the corresponding author upon reasonable request.

## Keywords

3D printing, gel, PEGgel, phase separation, shape-memory, soft matter

Received: January 26, 2023

Revised: March 8, 2023

Published online:

- [1] M. Y. Lin, H. J. Hu, S. Zhou, S. Xu, *Nat. Rev. Mater.* **2022**, *7*, 850.
- [2] J. Jiang, L. Han, F. Ge, Y. Xiao, R. Cheng, X. Tong, Y. Zhao, *Angew. Chem., Int. Ed.* **2022**, *61*, 202116689.
- [3] K. M. Herbert, H. E. Fowler, J. M. McCracken, K. R. Schlafmann, J. A. Koch, T. J. White, *Nat. Rev. Mater.* **2021**, *7*, 23.
- [4] M. E. Allen, J. W. Hindley, D. K. Baxani, O. Ces, Y. Elan, *Nat. Rev. Chem.* **2022**, *6*, 562.
- [5] Y. Fang, X. Yang, Y. Lin, J. Shi, A. Prominski, C. Clayton, E. Ostroff, B. Tian, *Chem. Rev.* **2022**, *122*, 5233.
- [6] Z. Zhu, D. W. H. Ng, H. S. Park, M. C. McAlpine, *Nat. Rev. Mater.* **2020**, *6*, 27.
- [7] C. Wang, T. Yokota, T. Someya, *Chem. Rev.* **2021**, *121*, 2109.
- [8] L. F. Hart, J. E. Hertzog, P. M. Rauscher, B. W. Rawe, M. M. Tranquilli, S. J. Rowan, *Nat. Rev. Mater.* **2021**, *6*, 508.
- [9] C. Xiang, Z. Wang, C. Yang, X. Yao, Y. Wang, Z. Suo, *Mater. Today* **2020**, *34*, 7.
- [10] X. Zhao, *Extreme Mech. Lett.* **2020**, *39*, 100784.
- [11] G. Su, J. Cao, X. Zhang, Y. Zhang, S. Yin, L. Jia, Q. Guo, X. Zhang, J. Zhang, T. Zhou, *J. Mater. Chem. A* **2020**, *8*, 2074.
- [12] M. K. Shin, G. M. Spinks, S. R. Shin, S. I. Kim, S. J. Kim, *Adv. Mater.* **2009**, *21*, 1712.
- [13] B. Kong, Y. Chen, R. Liu, X. Liu, C. Liu, Z. Shao, L. Xiong, X. Liu, W. Sun, S. Mi, *Nat. Commun.* **2020**, *11*, 1435.
- [14] K. Cui, Y. N. Ye, T. L. Sun, C. Yu, X. Li, T. Kurokawa, J. P. Gong, *Macromolecules* **2020**, *53*, 5116.
- [15] J. - Y. Sun, X. Zhao, W. R. K. Illeperuma, O. Chaudhuri, K. H. Oh, D. J. Mooney, J. J. Vlassak, Z. Suo, *Nature* **2012**, *489*, 133.
- [16] X. Y. Liu, J. Liu, S. T. Lin, X. H. Zhao, *Mater. Today* **2020**, *36*, 102.
- [17] F. Chen, D. Zhou, J. Wang, T. Li, X. Zhou, T. Gan, S. Handschuh-Wang, X. Zhou, *Angew. Chem., Int. Ed.* **2018**, *57*, 6568.
- [18] L. Addadi, S. Weiner, *Angew. Chem., Int. Ed. Engl.* **1992**, *31*, 153.
- [19] K. Guo, M. J. Buehler, *Matter* **2019**, *1*, 302.
- [20] K. Sato, T. Nakajima, T. Hisamatsu, T. Nonoyama, T. Kurokawa, J. P. Gong, *Adv. Mater.* **2015**, *27*, 6990.
- [21] R. Tamate, K. Hashimoto, T. Horii, M. Hirasawa, X. Li, M. Shibayama, M. Watanabe, *Adv. Mater.* **2018**, *30*, 1802792.
- [22] X. Liang, G. Chen, S. Lin, J. Zhang, L. Wang, P. Zhang, Y. Lan, J. Liu, *Adv. Mater.* **2022**, *34*, 2107106.
- [23] M. Wang, P. Zhang, M. Shamsi, J. L. Thelen, W. Qian, V. K. Truong, J. Ma, J. Hu, M. D. Dickey, *Nat. Mater.* **2022**, *21*, 359.
- [24] J. Huang, Y. Xu, S. Qi, J. Zhou, W. Shi, T. Zhao, M. Liu, *Nat. Commun.* **2021**, *12*, 3610.
- [25] Y. Xia, Y. He, F. Zhang, Y. Liu, J. Leng, *Adv. Mater.* **2021**, *33*, 2000713.

- [26] A. Lendlein, S. Kelch, *Angew. Chem., Int. Ed.* **2002**, *41*, 2034.
- [27] B. Zhang, H. Li, J. Cheng, H. Ye, A. H. Sakhaei, C. Yuan, P. Rao, Y. - F. Zhang, Z. Chen, R. Wang, X. He, J. Liu, R. Xiao, S. Qu, Q. Ge, *Adv. Mater.* **2021**, *33*, 2101298.
- [28] R. Liang, H. Yu, L. Wang, L. Lin, N. Wang, K.-u.-R. Naveed, *ACS Appl. Mater. Interfaces* **2019**, *11*, 43563.
- [29] P. R. A. Chivers, D. K. Smith, *Nat. Rev. Mater.* **2019**, *4*, 463.
- [30] T. J. Wallin, J. Pikul, R. F. Shepherd, *Nat. Rev. Mater.* **2018**, *3*, 84.
- [31] H. Yang, W. R. Leow, T. Wang, J. Wang, J. Yu, K. He, D. Qi, C. Wan, X. Chen, *Adv. Mater.* **2017**, *29*, 1701627.
- [32] M. Hua, S. Wu, Y. Ma, Y. Zhao, Z. Chen, I. Frenkel, J. Strzalka, H. Zhou, X. Zhu, X. He, *Nature* **2021**, *590*, 594.